Structures in the Coma of Comet C/NEAT (2001 Q4): Observations and Models

G. Borisov, **T. Bonev**

Institute of Astronomy, Bulgarian Academy of Sciences, BG-1784 Sofia, Bulgaria

Abstract. Comet C/NEAT (2001 Q4) was observed in three consecutive nights in May 2004 (19th, 20th and 21th) with the 2m Ritchey-Chretien-Coude telescope and the 2-Channel Focal Reducer at the Bulgarian National Astronomical Observatory (BNAO) – Rozhen. Narrow-band filters were used, centered on a blue and a red comets' continuum windows. The images exhibit shell-like structures. A dynamical Monte-Carlo model was developed and used to describe these structures. Comparison of modelled and observed shells suggests that the source region of the observed structures should be 10 times more active than the surrounding nucleus surface. The calibrated images were used to produce color maps of the dust. The color of the structure does not deviate strongly from the color of the ambient dust coma.

1 Introduction

Images of the near nucleus region of comets often show various structures. They are due to the nonuniform activity over the cometary nucleus surface. Different structures are produced depending on the physical parameters of the dust particles, the size of the active region, its coordinates on the nucleus surface, the particle size distribution, the rotational period and the orientation of the spin axis. One approach to understand the shape and surface density of these structures is to simulate them with numerical models which incorporate the above mentioned parameters.

The images of comet C/NEAT (2001 Q4), presented in this paper, show irregularities in the sunward hemisphere of the dust coma. After applying a numerical filter these irregularities appear as shell-like structures. We use a Monte-Carlo model to reproduce these structures and to derive values for the parameters responsible for the shape and brightness of the observed features. Our analysis shows that the source region of the observed structures should be about an order of magnitude more active than the surrounding nucleus surface. The color of the structures does not deviate strongly from the color of the ambient dust coma.

2 Instrumentation, Observations, and Data Reduction

2.1 Instrumentation

The observational material was obtained with the 2m RCC telescope at BNAO–Rozhen. The focal length of the RC–focus is $16\,000$ mm. This optical system gives a resolution of $12.8\,''/$mm. To increase the FOV and to decrease the focal ratio the 2 channel Focal Reducer Rozhen (*FoReRo2*) was used. Focal reducers are preferred devices for observing faint extended objects with low surface brightness. *FoReRo2* decreases the focal ratio from 1:8 to 1:2.8. In addition it gives the opportunity to take images simultaneously in two different wavelengths (*red* and *blue* channel).

Two filters for comet observations, centered at clean continuum windows (BC and RC), were used. BC is centered at 443 nm and has equivalent width of 3.9 nm and RC is centered at 642 nm and has equivalent width of 1.6 nm.

The detector in the blue channel is a CCD camera Photometrics, CE200A-SITe, comprising 1024×1024 px^2. In the red arm a VersArray 512B camera is used, comprising 512×512 px^2. Both CCD cameras have square pixels of size $24\,\mu m$, and are cooled with liquid nitrogen. With this cameras and the described optical system the spatial scale is $0.89\,''/$px. A mean seeing of about $2''$ (which is usual for BNAO – Rozhen) is distributed over about two pixels, i.e. the optical system works with optimal sampling (Theorem of Nyquist or Shannon [10]).

2.2 Description of the observations

The comet was observed in three consecutive nights near the perihelion. Table 1 contains the heliocentric and geocentric distances, the phase angle (S-T-O), the position angles of the extended Sun–target radius vector (PsAng) and the negative of the target's heliocentric velocity vector (PsAMV).

Table 1. Conditions during the observations.

Date	r	Δ	S-T-O	PsAng	PsAMV
19 May 2004	0.964	0.525	79.69	101.8	190.8
20 May 2004	0.966	0.549	78.60	101.4	190.4
21 May 2004	0.968	0.577	77.38	100.9	189.9

2.3 Data reduction

After the standard CCD image data reduction, the images of the comet were calibrated to fluxes. The CCD devices are linear detectors [8]. Therefore the conversion from registered signal to absolute values, fluxes, is made with the linear transformation $F_{com} = Q_\lambda \times S_{com}$, where F_{com} and S_{com} are the derived

flux and the signal measured in the image of the comet. Spectrophotometric standard star measurements were used to derive the linear coefficients, $Q_\lambda = F_*/S_*$, where F_* is the flux of the star, taken form [6, 7], and S_* is the signal measured in its image. The standard stars were observed at the same airmass as the comet. Following values of the coefficients transforming to fluxes were calculated: $Q_{443} = 1.35 \times 10^{-14}$ erg cm^{-2} sec^{-1} Å^{-1}/(ADU/s) and $Q_{642} = 6.03 \times 10^{-15}$ erg cm^{-2} sec^{-1} Å^{-1}/(ADU/s). Finally the images were calibrated to mean solar disk intensity and Af introduced by [1].

$$Af = \frac{F_{com}}{F_\odot} \left(\frac{r_h}{1AU}\right)^2 \left(\frac{2\Delta}{\rho}\right)^2,\tag{1}$$

where A is the Bond albedo and f is the filling factor.

One of the ways for setting up restrictions on the properties of the particles in the cometary dust coma is to obtain the "colour" of the dust coma. This colour is defined as *the normalized gradient of the scattering efficiency of the dust coma in a given wavelength interval* $[\lambda_1, \lambda_2]$, and has following form [5]: $C_{(\lambda_1, \lambda_2)} = (\partial F/\partial \lambda)/F_{mean}$.

3 Mean Radial Flux and Color Maps

Near the nucleus (several hundreds of kilometers) the contribution of the radiation pressure to the velocity of the dust particles is less than their terminal velocity and $V_d \approx$ const. can be assumed. Thus, in the case of radial and isotropic outflow of dust the radial density distribution is $n(R) = Q_d/(4\pi R^2 V_d)$ (mass conservation), where Q_d is the dust production rate. Integration along the line of sight gives the observed column densities, $N(\rho) = Q_d/(4\rho V_d)$. From the relation $N(\rho) \propto \rho^{-1}$ follows that the product of Af and ρ should be constant. Mean radial profiles, calibrated in terms of Af, are presented in the left panel in Figure 1 and compared to the theoretically expected ρ^{-1} profiles. The $Af\rho$ values, derived from these profiles, are shown in the corresponding panels. Table 2 contains $Af\rho$ values for all observations. From the calibrated images the color maps are prepared. The mean color of the dust coma is 43%. There is an indication of slightly reddening in the region of the shell-like structures (see right panel in Figure 1).

Table 2. $Af\rho$ values for all images and all days.

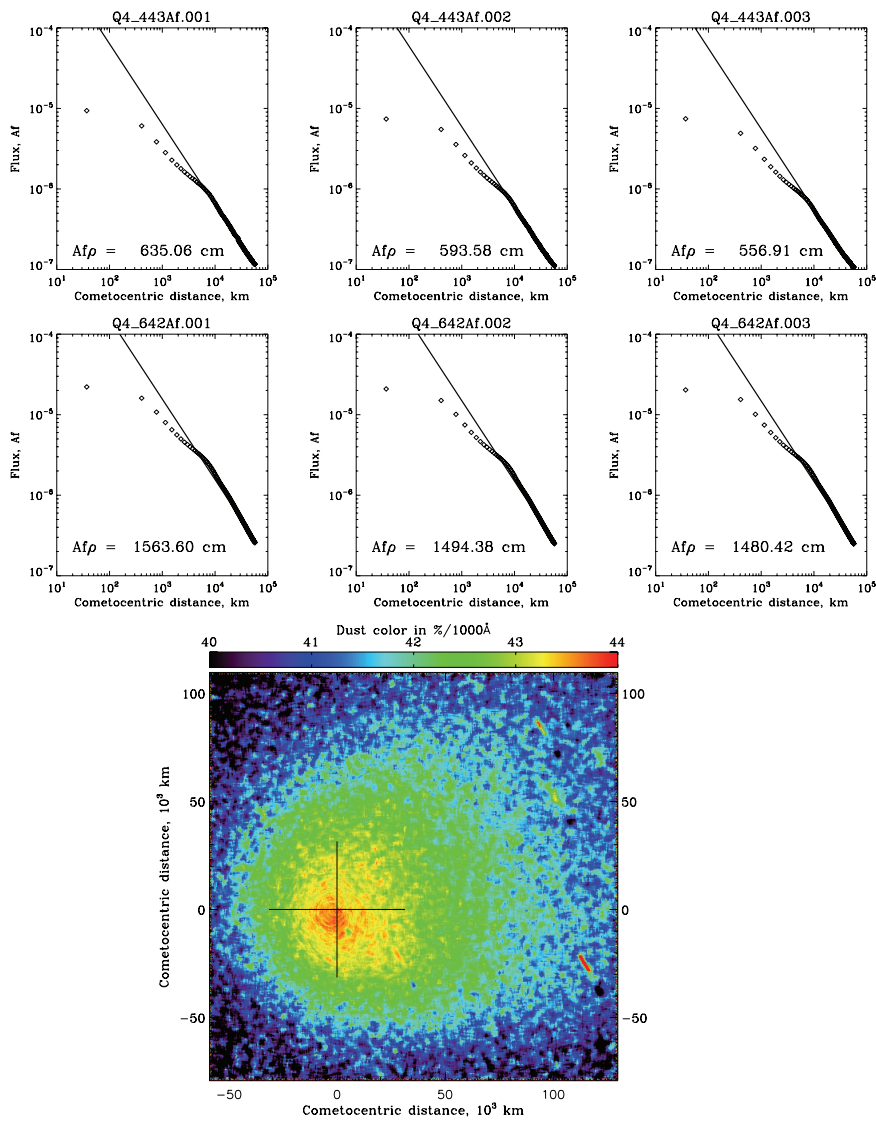| Date	$Af\rho_{443}$, [cm]	$Af\rho_{642}$, [cm]	Date	$Af\rho_{443}$, [cm]	$Af\rho_{642}$, [cm]
19 May 2004	620.63	1963.73	20 May 2004	923.18	1892.65
19 May 2004	484.31	1465.99	20 May 2004	915.71	1810.64
19 May 2004	-	1587.64	21 May 2004	635.06	1563.60
19 May 2004	-	1767.62	21 May 2004	593.58	1494.38
20 May 2004	1065.13	1988.65	21 May 2004	556.91	1480.42

Figure 1. Af vs ρ plots and calculated $Af\rho$ values – upper panel, and color map – down panel, for 21 May 2006

4 Image Processing Techniques Enhancing Coma Structures in the Coma

Using the expected canonical shape of the coma we can remove the bulk brightness by dividing the observed image by a synthetic one, which follows the $1/\rho$
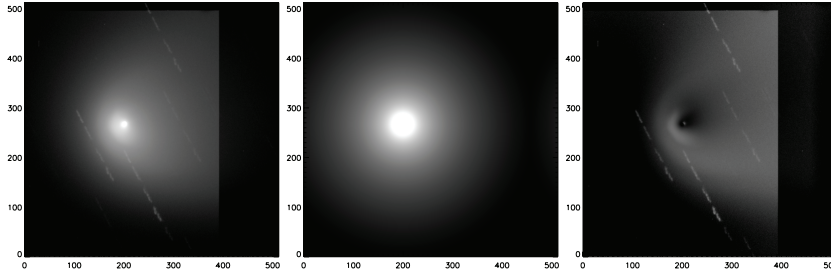
Figure 2. Left: raw image, middle: synthetic $1/\rho$ image, right: the ratio between the *left* and *middle* images.

law. Figure 2 illustrates the application of this image enhancing technique. The left panel in this figure contains the original image, in the middle panel the corresponding $1/\rho$–image is shown, and the right panel presents the resultant ratio with the clearly enhanced shell-like structures.

5 Dynamical Simulations of the Observed Structures

5.1 Basics of cometary dust dynamics

The dust coma consist of solid particles with dimensions from below micrometers to about 1 cm. In his model Whipple [11] has shown that the larger particle which can be emitted is about 1 cm.

The forces, which are acting on the dust particles after they leave the nucleus, are expressed as followed [3]:

$$1 - \mu = \beta = \frac{F_{\text{rad}}}{F_{\text{grav}}},$$

$$F_{\text{rad}} = \frac{Q_{\text{pr}}}{c}\left(\frac{E_{\text{s}}}{4\pi r_{\text{h}}^2}\right)\frac{\pi a^2}{4}, \quad F_{\text{grav}} = \frac{GM_{\odot}}{r_{\text{h}}^2}\left(\frac{\rho_{\text{d}}\pi a^3}{6}\right) \tag{2}$$

$$\beta = C\left(\rho_{\text{d}}a\right)^{-1}, \quad C = \frac{3Q_{\text{pr}}E_{\text{s}}}{8\pi cGM_{\odot}} = 1.19 \times 10^{-4}Q_{pr}, g\,\text{cm}^{-2}$$

where E_{s} is the Solar luminosity , c – the velocity of light, a – particles' radii, ρ_{d} – their density, r_{h} – the heliocentric distance, $M_{\odot}$ – Solar mass, G – gravitational constant, Q_{pr} – the Solar pressure efficiency.

From space missions, which collect dust particles in near Earth environment, we know that $\rho_d \in [1, 3]\,\text{g}\,\text{cm}^{-3}$. The probability of an arbitrary selected particle to be in an infinity small interval from a to $a + da$ is the particles size distribution (PSD), $g(a)$. The PSD should satisfy $\int_0^{\infty} g(a)\mathrm{d}a = 1$. Analysis of the data from space missions to comet Halley have shown that the PSD can be described

with a power law $g(a) \propto a^{-\nu}$. Results for the power index ν derived from the spacecraft *VEGA2* are presented in Table 3.

Table 3. Power index of the PSD law derived from the spacecraft *VEGA2*

ν	$\rightarrow$	a
2.00	$\rightarrow$	$a < 0.62\,\mu\mathrm{m}$
2.75	$\rightarrow$	$0.62\,\mu\mathrm{m}< a < 0.62\,\mu\mathrm{m}$
3.00	$\rightarrow$	$a > 6.2\,\mu\mathrm{m}$

The gas drag force accelerates particles of different sizes to different velocities. The terminal velocity of the gas–dust interaction is the initial velocity in the dynamical models. Often [4] following relation is used for the dependence of the initial velocity:

$$V_d = V_0 \left(\frac{a_0}{a}\right)^{-\gamma}, \text{ where } V_0 = 500 \text{ m/s, } a_0 = 1\,\mu\mathrm{m}, \gamma = \frac{1}{2} \qquad (3)$$

5.2 The Monte–Carlo model

For the description of the shell-like features a Monte-Carlo model, based on Finson-Probstein theory of dust particles dynamics, is developed. The size of the active region, its coordinates on the nucleus surface, and the range of the dust particles' sizes were found by trial and error. Fixed values of the particle size distribution, the rotational period and the orientation of the rotation axis were adopted. The model is based on a coordinate system centered on the comet's nucleus, The x-axis is orientated to the Sun, the y-axis is perpendicular to x in counterclockwise direction in the plane of the comet orbit, and the z-axis complements the rectangular coordinate system. By trail and error we found that the observations are well reproduced when the z-axis is close to the comet spin axes.

Let's assume that a small active region exists on the nucleus surface at coordinates θ and φ. If a dust particle escapes from this active region, its position after a time interval t will be described by:

$$\begin{aligned}
x &= V_d t \sin\varphi \cos\theta - \tfrac{1}{2}\alpha t^2 \\
y &= V_d t \sin\varphi \sin\theta \\
z &= V_d t \cos\varphi,
\end{aligned} \qquad (4)$$

where α is the accelerations of the particles. Because we are considering short living structures we are using constant accelerations in an inertial reference frame. The released dust particles are uniformly distributed over this region. The initial coordinates are described by:

$$\begin{aligned}
\varphi &= \varphi_0 - \tfrac{\mathrm{d}\varphi}{2} + R_i \mathrm{d}\varphi \\
\cos\theta &= \cos\left(\theta_0 - 2\pi\tfrac{t}{P} - \tfrac{\mathrm{d}\varphi}{2}\right) + R_i \mathrm{d}\cos\theta,
\end{aligned} \qquad (5)$$

where R_i is a set of random numbers ($R \in [0, 1]$). All particles of various sizes, released at different times, form a 3D data array. Finally, their contributions are integrated along the line of sight to obtain a 2D image, which can be compared to the observed image containing coma structures:

$$B_{xy} = C \int\limits_{z_1}^{z_2} \int\limits_{a_{min}}^{a_{max}} N(x, y, z, a) \, g(a)\pi a^2 \mathrm{d}a\mathrm{d}z, \quad C = \left(\int\limits_{a_{min}}^{a_{max}} g(a)da \right)^{-1}, \quad (6)$$

where $N(x, y, z, a)$ is the result of the Monte-Carlo calculation, namely the number of particles of size a at coordinates (x, y, z), and z_i are the limits of the 3D data grid along the line of sight. In Figure 3 one can see an example of a simulated jet produced from an active region with latitude on the nucleus $45°$. The comet is rotating for half a comet day. The three panels show projections along three perpendicular lines of sight.
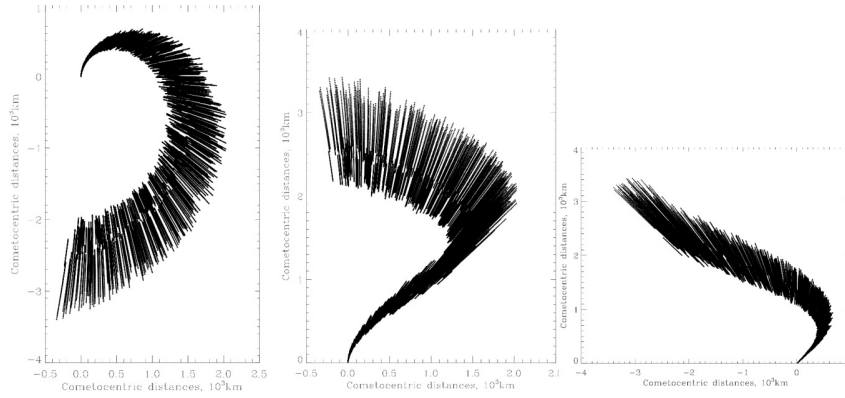

Figure 3. From left to right: projections of a modeled jets onto the $X - Y$, $X - Z$ and $Y - Z$ planes, respectively

The left panel in Figure 4 shows a processed image of comet C/NEAT (2001 Q4), obtained on 19 May 2004. A simulated image, which roughly reproduces the observed structures, is presented in the right panel in Figure 4. This simulation is created by ejecting 101 particles every 12 second over the time interval of 4 comet days (rotation period of the comet is P=22h). The parameters used for this simulation are given in Table 4.

Table 4. Monte-Carlo model parameters.

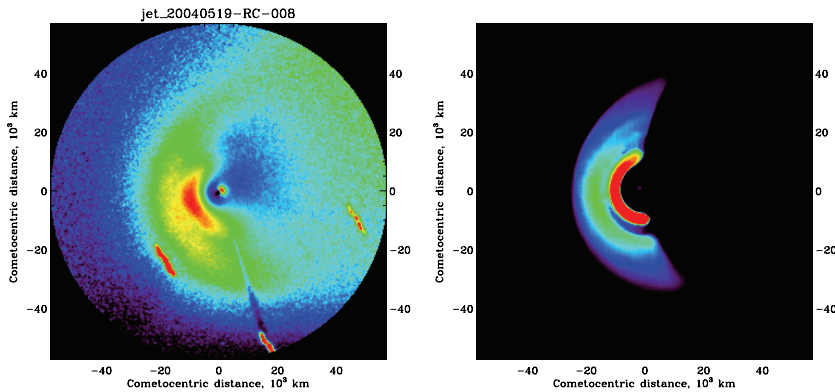| θ	φ	$\mathrm{d}\varphi$	a	Δt	P
90	90	5	40–90 μm	12 sec	22 h

Figure 4. Observed (left panel) and simulated (right panel) shell-like structures.

The measured flux in the observed shell-like structure is about 2 times greater in comparison to the flux of the ambient dust coma. Our simulation shows that the structures are best reproduced with an active region having an angular size of 5∘. This means that the active area is expended only over about 0.06% of the nucleus surface.

6 Conclusions

1. Observations of the dust coma of comet C/NEAT (2001 Q4) are obtained.

2. The images are absolutely calibrated and $Af\rho$ values and dust color are calculated.

3. The dust coma is characterized by the presence of discrete structures.

4. The observed structures are enhanced over the ambient dust coma with application of a suitable numerical radial filter.

5. A Monte-Carlo model is developed and the structures are modeled and compared with the original data.

6. The contribution of the structures to the brightness of the dust coma is evaluated.

References

[1] M.F. A'Hearn, *et al.* (1984) *AJ* **89** 579.
[2] T. Farnham, *et al.* (2001) *Science* **292** 1348.

[3] M. Finson, R. Probstein (1968) *AJ* **154** 327.

[4] M. Fulle (2000) *Icarus* **145** 239.

[5] D. Jewitt, K.J. Meech (1986) *AJ* **310** 973.

[6] Mario Hamuy *et al.* (1992) *PASP* **104** 533.

[7] Mario Hamuy *et al.* (1994) *PASP* **106** 566.

[8] S. Howell (2000) "*Handbook of CCD Astronomy*" Cambridge University Press.

[9] S. Larson, Z. Sekanina (1984) *AJ* **89** 571.

[10] Pierre Lèna (1988) *Observational Astrophysics*, Springer-Verlag Berlin Haidelberg.

[11] F. Whipple (1951) *AJ* **113** 464.